frontiers | Frontiers in Energy Research

TYPE Original Research
PUBLISHED 29 August 2022
DOI 10.3389/fenrg.2022.975602

OPEN ACCESS

EDITED BY
Yinbo Zhou,
Henan University of Engineering, China

REVIEWED BY
Ming Ji,
China University of Mining and Technology, China
Xin Ding,
Liaoning Technical University, China

*CORRESPONDENCE
Wang Yin,
495981609@qq.com

SPECIALTY SECTION
This article was submitted to Carbon Capture, Utilization, and Storage, a section of the journal Frontiers in Energy Research

RECEIVED 22 June 2022
ACCEPTED 29 July 2022
PUBLISHED 29 August 2022

CITATION
Yin W, Bin Z, Zhigang D, Kun L and Hongwei W (2022), Research on behavior of underground pressure in shallow coal seam with three-face goaf working face.
Front. Energy Res. 10:975602.
doi: 10.3389/fenrg.2022.975602

Research on behavior of underground pressure in shallow coal seam with three-face goaf working face

Wang Yin[1,2]*, Zhao Bin[2], Deng Zhigang[2], Lv Kun[2] and Wang Hongwei[2]

[1]School of Energy and Mining Engineering, China University of Mining and Technology (Beijing), Beijing, China, [2]China Coal Research Institute, Beijing, China

During the mining process of coal mines, coal pillars are often formed in the goaf on three sides, and the stress behavior of coal seams has a significant impact on the safety of coal mines. The upper part of panel 3104 of Xinwang Coal Mine is the room-pillar goaf of the 2# coal seam, and the lower part is the goaf of the 7# coal seam. The same coal seam is adjacent to the goaf of panel 3102. Therefore, there are hidden dangers for safe mining in panel 3104 affected by the goaf on three sides. Through FLAC^{3D} numerical simulation, on-site Pasat-M detection, microseismic monitoring, and support resistance measurement, the stress distribution law of surrounding rock in the working face is analyzed. The following conclusions are obtained. There are several high wave velocity stress concentration areas in the coal body of 3104 working face. During the mining of the working face, the mining influence 90m in front of the working face began to spread to the area of the left coal pillar, and the vertical stress at the left coal pillar began to increase. Stress concentration appears in 0–20m strata at the top of 3# coal seams. At the top of a 3# coal seam, the vertical stress concentration coefficient can reach 2 in the range of 4–12m. The influence range of 3104 working face mining advance can reach 200m. Under the influence of mining, a large number of microseismic events occurred at 160m above and 150m below 3# coal seam. This law has reference value for the mining strata behaviors of coal seams under similar conditions.

KEYWORDS

room and pillar mining, microseismic monitoring, underground pressure, three-face goaf, pasat-M detection

Introduction

In the early stage of the Datong mining area, a series of problems were left due to unreasonable mining arrangements, such as room-pillar mining, above-gob mining, and headspace mining, which seriously affected the safe and efficient mining of working face.

Domestic experts and scholars have done a lot of research on room-pillar mining and above-gob mining in the Datong mining area. Feng et al. studied the stress distribution law of the floor in the cutting pillar mining over the goaf, and concluded that the influence of mining stress is the main reason for the instability of the residual coal pillar in the goaf and the irregular collapse of the overburden (Feng et al., 2014; Wang, 2019). Tu et al. analyzed the roof control technology of near-distance fully mechanized coal seam mining under shallow buried chamber column goaf employing similarity simulation, numerical simulation, and field measurement methods (Tu et al., 2011; Li Z. et al., 2020; Yu et al., 2021). Based on this, they took control and prevention measures, such as blasting and releasing pressure of residual coal pillar, filling coal room with sand injection, and reasonable control of mining height, and realized safe and efficient production of working face. Xie et al. established a mathematical analysis model of the roof—coal pillar group system in the roof-pillar goaf of a shallow buried coal seam (Xie, 2014; Kai et al., 2017; Wang et al., 2020). They calculated the stability of the roof pillar group system of room pillar goaf in Kuiwu coal mine in Ordos area iteratively, which provided theoretical support for the stability evaluation of the roof pillar group system of room pillar goaf in a shallow coal seam. Fu et al. studied the stability of coal pillars in room-pillar goaf under shallow mining geological conditions by using the theory of mine rock mechanics and finite element strength reduction (Fu et al., 2011; Zhang et al., 2013; Du and Huang, 2022). Wang et al. took Shigegetai coal mine 31201 working face in the Shendong mining area as the research object, using the field measurement and theoretical analysis method to study the mechanism of abnormal mining pressure under unstable coal pillars (Wang et al., 2016; Chai et al., 2020).

Although a large number of scholars have carried out a large number of studies on the overlying room-pillar mining, above goaf mining, and adjacent sequential mining, the study on the working face affected by the three aspects of goaf at the same time is insufficient (Meng et al., 2007; Kong et al., 2016; Jiang et al., 2017; Zhang et al., 2018; Li et al., 2019; Liu et al., 2019; Li J. Z. et al., 2020). When there are three goaf in the working face space structure, the strata behaviors are more intense, so it is easier to cause the problems of support overload, wall caving, and support failure. Therefore, through the method of combining underground measurement and numerical simulation, taking the 3104 working face of Xinwang Coal Mine as the engineering background, this paper studies the law of strata behaviors of panel 3104 with a three-face goaf working face. The research results can provide a reference for similar mining in the future.

Project overview

Xinwang Coal Mine is located in Xinrong District, Datong City, Shanxi Province. Xinwang Coal Mine is now mainly mining 3# coal seams. The thickness of the coal seam is 1.6–1.8 m, with an average of 1.7 m. The occurrence of coal seams is relatively stable, the average dip angle of coal seams is 3°, and the hardness coefficient f = 3-4, which belongs to the hard coal seam.

The distance between 3# coal seam and 2–3# coal seam is 1.0–2.8 m, the thickness of 2–3# coal seam is 1.2–1.8m, and the distance between 2 and 3# coal seam and 2–2# coal seam is 1.0–2.0 m. The basic top thickness of 2 # coal seams is about 120m, which is composed of cemented siltstone, coarse sandstone, and conglomerate, respectively. The 7# coal seam and the 11# coal seam at the bottom of 3# coal seam have been mined out. The average distance between 3# coal seam and a 7# coal seam is 40.2m, and the average distance between 11# coal seam and 3# coal seam is 80.5 m. 3# coal seam is currently mining panel 3104. The upper part of 3104 working face is the room-pillar goaf left by 2# coal seam, and the coal pillars are mainly distributed between 280 and 300m. The lower part of panel 3104 is 7# coal seam goaf. The north of panel 3104 is the goaf of panel 3102.

Under the influence of mined-out areas on the overlying, underlying, and north side of panel 3104, the mining strata behaviors of the working face appear strongly. The panel layout and the influence area of the overlying coal pillar are shown in Figure 1.

Analysis of the main controlling factors of the surrounding rock stress around the panel

The degree of mine pressure in 3104 working face is affected by the lateral stress in goaf, the concentrated coal pillar in the overlying goaf, and the underlying goaf mining. Therefore, PASAT-M and microseismic monitoring were used to monitor the main influencing factors of surrounding rock stress in panel 3104 (Song et al., 2021; Wang et al., 2022).

PASAT-M microseismic detection analysis

PASAT-M microseismic detection system is mainly based on seismic wave tomography to complete the detection of the target rock mass (Lin et al., 2014; Liang, 2017). PASAT-M can obtain the distribution image of seismic wave velocity or attenuation coefficient of seismic wave inside the target rock mass through the change of seismic wave time or energy through the medium.

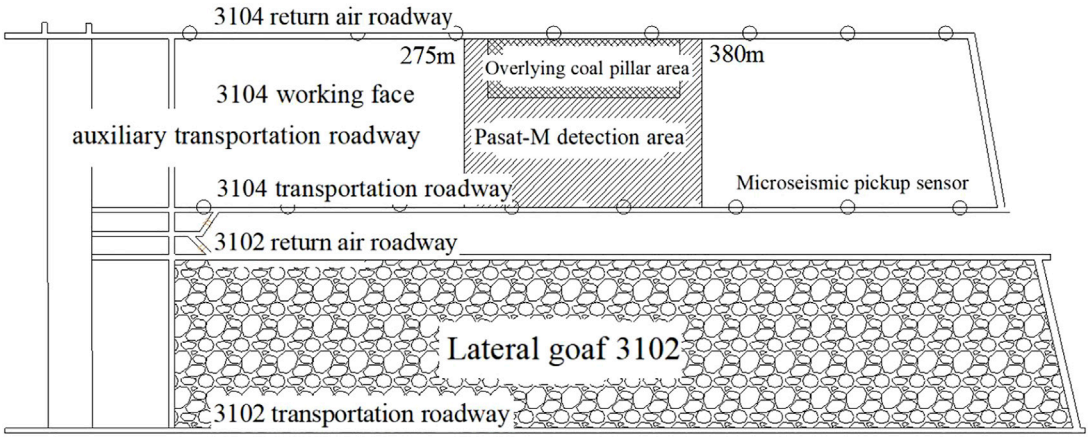

FIGURE 1
Mining engineering plan.

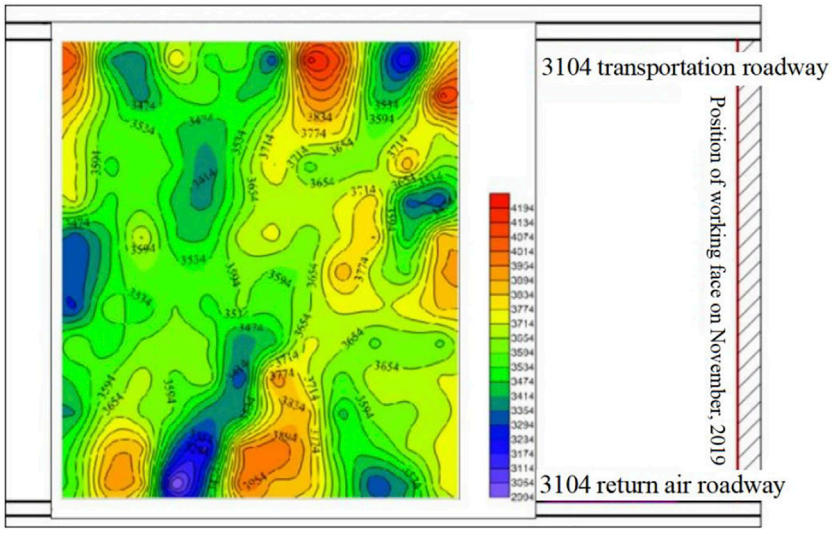

FIGURE 2
Cloud image of wave velocity distribution in the detection area (m/s).

Based on the positive correlation between wave velocity field and stress field, the distribution of typical abnormal regions such as geological structure, stress anomaly area, and thickness change in target rock mass is deduced. To clarify the stress distribution characteristics of the coal body in panel 3014, PASAT-M test was conducted on the working face. The detection area is shown in Figure 1, and the wave velocity distribution cloud diagram in the detection area is shown in Figure 2.

The wave velocity field in this region is at a relatively high level as a whole. The wave velocity is mainly 3400–3700 m/s, and the highest and lowest wave velocities are 4194 m/s and 2994 m/s, respectively. The high wave velocity zone of the transportation roadway is located at 275–280 m, 340–350 m, and 370–380 m, while the low wave velocity zone is located at 295 m, 330 m, and 360–370 m. The high wave velocity zone of the return air roadway groove is located at 285–295 m and 320–340 m, while the low wave velocity zone is located at 300–310 and 360 m. There are five high wave velocity areas between the two roadways, and the wave velocity is mainly 3900–4200 m/s. Since there is no fault development in this area, it can be considered that the high stress in this area is superimposed by the stress of the coal pillar of the overlying no.2 coal seam goaf and the stress

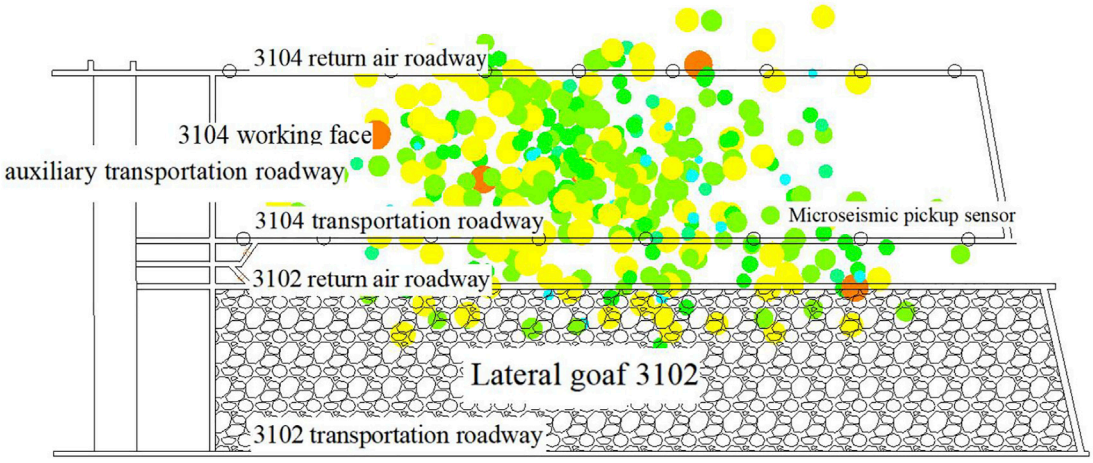

FIGURE 3
The plane distribution range of microseismic events.

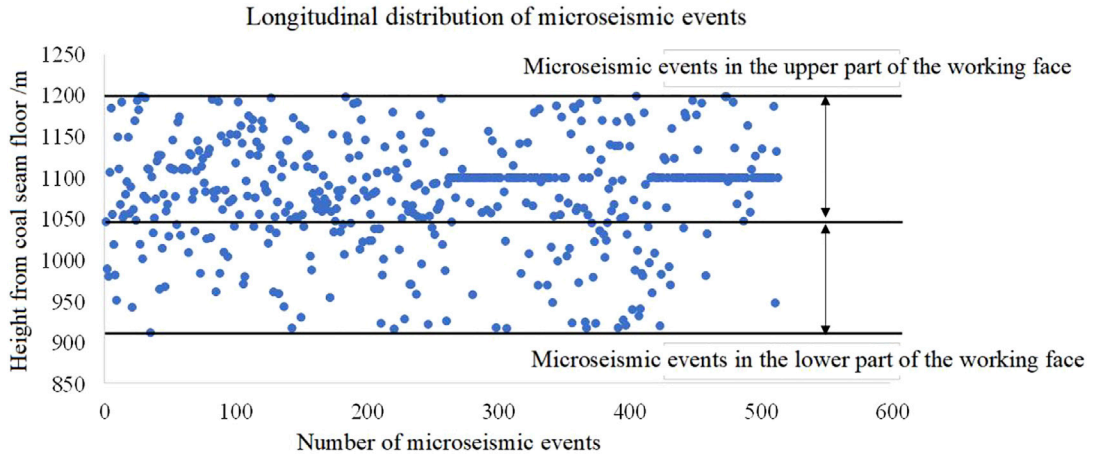

FIGURE 4
Longitudinal spatial distribution range of microseismic events.

of the side goaf of the 3102. It can also be seen from the distribution of PASAT-M high wave velocity that the concentrated stress generated by the coal pillar in the goaf of the overlying No.2 coal seam has a greater influence on the working face than the side stress in the goaf of 3102 coal seam.

Microseismic monitoring results and analysis

The KJ768 high precision microseismic monitoring system was used to monitor coal and rock vibration in 3104 working face. Source distribution positions during monitoring are shown in Figure 3 and Figure 4.

According to the analysis of microseismic monitoring results, the following conclusions are drawn. The leading influence range of 3104 working face is 200m. Microseismic events are concentrated in the range of 280–380 m overlying coal pillars. The failure height of the overlying rock of the working face can reach 160m. There are a few microseismic events within 150 m of the goaf. It shows that under the influence of the three mined-out areas, the coal seam mining in the middle of the near-room mining area will have a great influence on the mining range. The distribution density of microseismic events in 7# and 11# coal

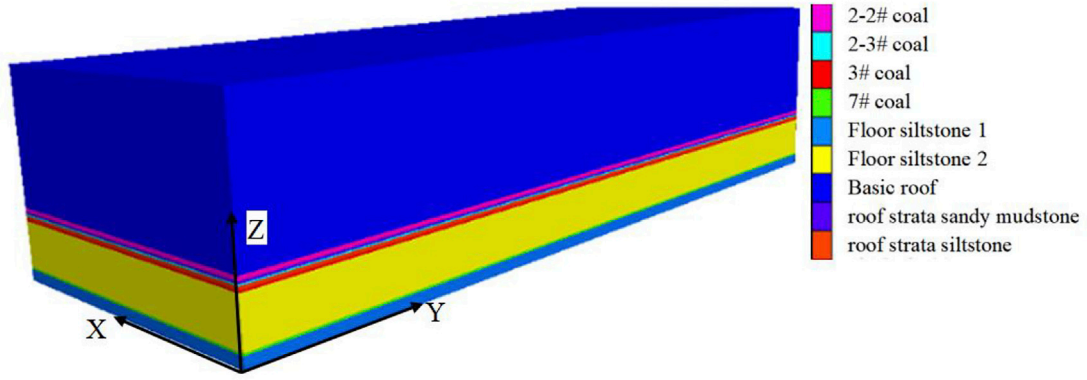

FIGURE 5
Three-dimensional numerical model.

seams at the bottom of a 3# coal seam is relatively small. The density distribution of microseismic events is large in the low and high basic roof of the overlying strata of the 3# coal seam. This shows that the 7# coal seam and the 11# coal seam have little influence on the safety mining of 3# coal seam, and the upper 2# coal seam and the lateral goaf 3102 have a great influence on the safety mining of the 3# coal seam.。

The following conclusions can be deduced from the characteristics of pillar mining and microseismic monitoring results in the near goaf. In room-pillar mining, the pillar supports the basic roof and overburden load. When mining the 3# coal seam, the overlying rock strata of the upper 2# coal seam will be partially destroyed and acted on the coal pillar of 2# coal seam. Coal pillar movement will change the stress of the underlying rock, resulting in the accumulation of stress in panel 3104. At the same time, under the influence of goaf 3102 on the side, the superposition of advanced mining stress and lateral stress is formed in front of 3104's working face to accumulate and release energy.

To sum up, the concentrated coal pillar of the overlying 2–2# coal seam has the greatest influence on the safe mining of panel 3104. Therefore, it is necessary to carry out further targeted research on the influence of concentrated coal pillars on the overlying goaf.

Stress distribution of the coal pillar above the panel

Taking the 3104 working face of Xinwang Coal Mine as the research object, the FLAC3D numerical model is established. The model covers panel 3104 and its section coal pillars in the horizontal direction, and the vertical direction is from the 7# coal floor siltstone to the 2–2# coal roof strata. The length of the model in the *X*, *Y* and *Z* directions is 120, 580, and 300 m, respectively. A vertical stress of 2 MPa was applied above the model, and the lateral pressure coefficient was 1.0. Fixed displacements were applied to the front, rear, left, right, and bottom of the model to define the boundary, and the Mohr-Coulomb constitutive relation was used as the model operation criterion (Gao, 2019; Yang et al., 2019; Xue et al., 2020; Yu et al., 2020; Zhou et al., 2020; Li et al., 2022). The three-dimensional numerical model is shown in Figure 5, and the rock mechanical parameters are shown in Table 1.

During the model calculation, the initial stress balance of the model is carried out first, and then the 2–2# coal seam covering panel 3104 is excavated. The room-pillar mining method is adopted, and three 20m concentrated coal pillars are left. After the 2–2# coal seam is excavated and the balance is calculated, panel 3104 is excavated, as shown in Figure 6.

Stress distribution law of surrounding rock in overlying strata of 3# coal seam

Figure 7 shows the cloud diagram of vertical stress distribution at 0m above the roof of a 3# coal seam. It can be seen from Figure 7 that when 2–2# coal is mined, there is stress concentration in the rock layer below the concentrated coal pillar. The vertical stress is 7.5–9.22 MPa, the vertical stress of the original rock is 5.4MPa, and the stress concentration coefficient is 1.39–1.71. The vertical stress of the surrounding rock under the chamber column is 6.0–9.0 MPa, and the stress concentration coefficient is 1.11–1.67.

Figure 8 shows the cloud diagram of vertical stress distribution at 2m above the roof of 3#coal seams. Figure 8 shows that the vertical stress of surrounding rock under a concentrated coal pillar is 8.0–9.77 MPa, the vertical stress of raw rock is 5.37 Mpa, and the stress concentration coefficient reaches 1.49–1.82. The vertical stress of the surrounding rock

TABLE 1 Mechanical parameters of model rock strata.

Lithology	Thickness	Density kg/m3	Bulk modulus/GPa	Shear modulus of elasticity/GPa	Cohesionvalue/ MPa	Angle of internal friction	Tensile strength /MPa
Basic roof	201.40	2700	6.23	3.43	14.0	45	8.22
2-2# coal seam	6.67	1300	3.71	1.00	6.0	41	1.20
Roof sandy mudstone	1.75	2580	4.30	2.42	12.0	42	2.95
2-3# coal seam	1.75	1300	3.71	1.00	6.0	41	1.20
Roof siltstone	6.72	2650	5.94	3.25	13.3	43	7.00
3# coal seam	1.70	1300	3.71	1.00	6.0	41	1.20
Floor siltstone 2	62.11	2650	5.94	3.25	13.3	43	7.00
7# coal seam	4.56	21300	3.71	1.00	6.0	41	1.20
Floor siltstone 1	13.33	2650	5.94	3.25	13.3	43	7.00

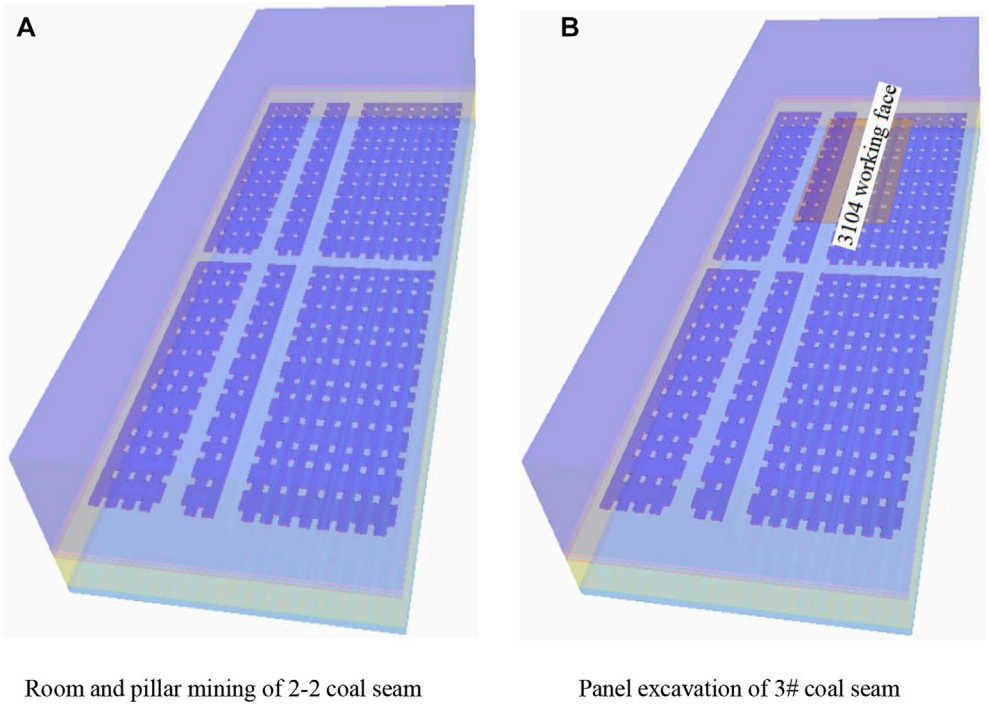

FIGURE 6
Mining plan of room and pillar mining. **(A)** Room and pillar mining of 2-2 coal seam **(B)** Panel excavation of 3# coal seam

under the chamber column is 6.0–9.5 MPa, and the stress concentration coefficient is 1.12–1.77.

Figure 9 shows the cloud diagram of vertical stress distribution at 4 m above the roof of 3#coal seams. Figure 9 shows that the vertical stress of surrounding rock under a concentrated coal pillar is 8.0–10.0MPa, the vertical stress of raw rock is 5.32 MPa, and the stress concentration coefficient reaches 1.50–1.88. The vertical stress of the surrounding rock under the chamber column is 6.0–12.0 MPa, and the stress concentration coefficient is 1.13–2.26.

Figure 10 shows the cloud diagram of vertical stress distribution at 6 m above the roof of 3#coal seams. Figure 7 shows that the vertical stress of surrounding rock under a concentrated coal pillar is 8.0–11.0MPa, the vertical stress of

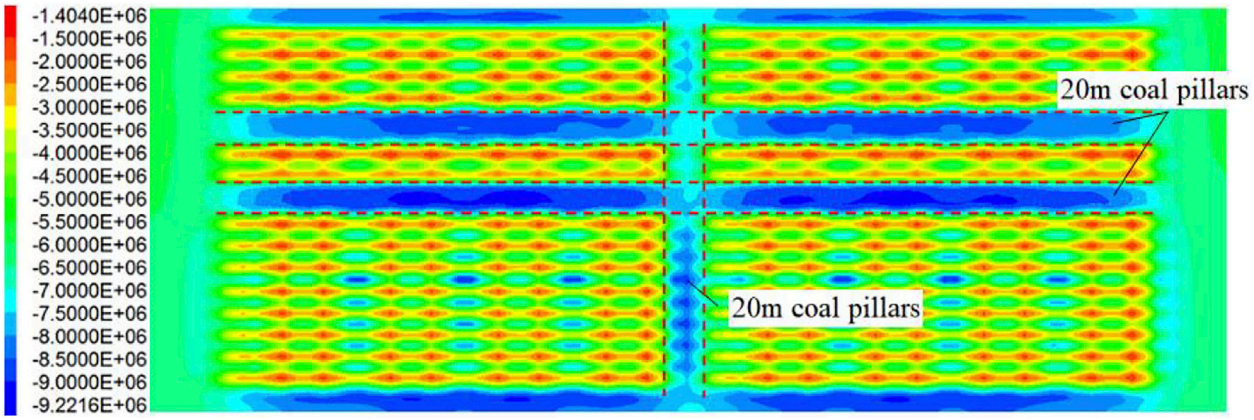

FIGURE 7
Vertical stress distribution of strata at 0 m on top of 3# coal seam (Pa).

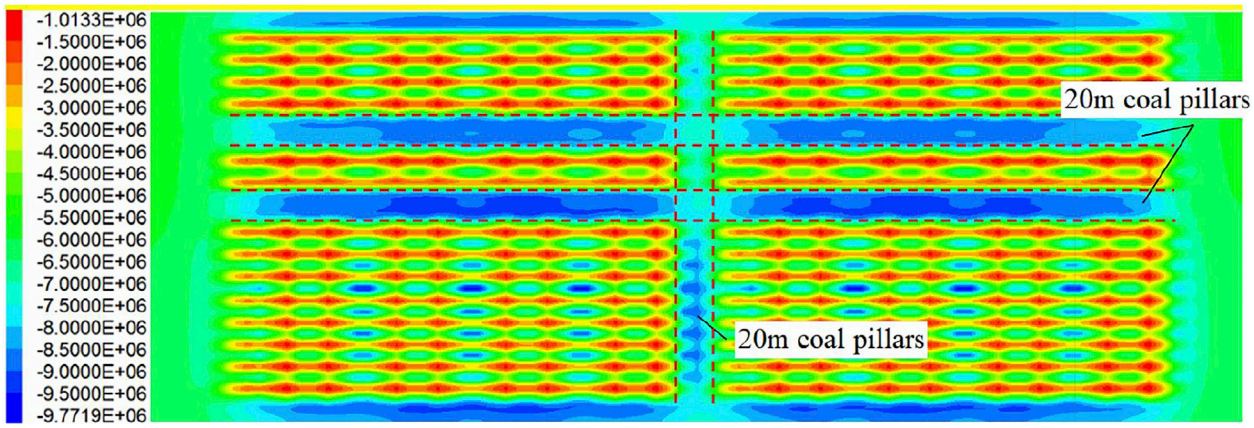

FIGURE 8
Vertical stress distribution of strata at 2 m on top of 3# coal seam (Pa).

raw rock is 5.28 MPa, and the stress concentration coefficient reaches 1.52–2.08. The vertical stress of the surrounding rock under the chamber column is 6.0–17.0MPa, and the stress concentration coefficient is 1.14–3.22.

Figure 11 shows the cloud diagram of vertical stress distribution at 8 m above the roof of 3#coal seams. Figure 11 shows that the vertical stress of surrounding rock under a concentrated coal pillar is 4.5–12.5 MPa, the vertical stress of raw rock is 5.25 MPa, and the stress concentration coefficient reaches 1.42–2.38. The vertical stress of the surrounding rock under the chamber column is 15.0–30.0 MPa, and the stress concentration coefficient is 2.86–5.71.

Figure 12 shows the cloud diagram of vertical stress distribution at 10m above the roof of a 3# coal seam. Figure 8 shows that the vertical stress of surrounding rock is 7.5–11.0 MPa, the vertical stress of original rock is 5.21MPa, and the stress concentration coefficient is 1.44–2.11. The vertical stress of the surrounding rock is 6.0–16.0 MPa and the stress concentration coefficient is 1.15–3.07.

Figure 13 shows the cloud diagram of vertical stress distribution at 12 m above the roof of 3#coal seams. Figure 13 shows that the vertical stress of surrounding rock under a concentrated coal pillar is 8.0–10.0MPa, the vertical stress of raw rock is 5.17 MPa, and the stress concentration coefficient reaches 1.55–1.93. The vertical stress of the surrounding rock under the chamber column is 6.0–11.0 MPa, and the stress concentration coefficient is 1.16–2.13.

Figure 14 shows the cloud diagram of vertical stress distribution at 14 m above the roof of 3#coal seams. Figure 14 shows that the vertical stress of surrounding rock under a

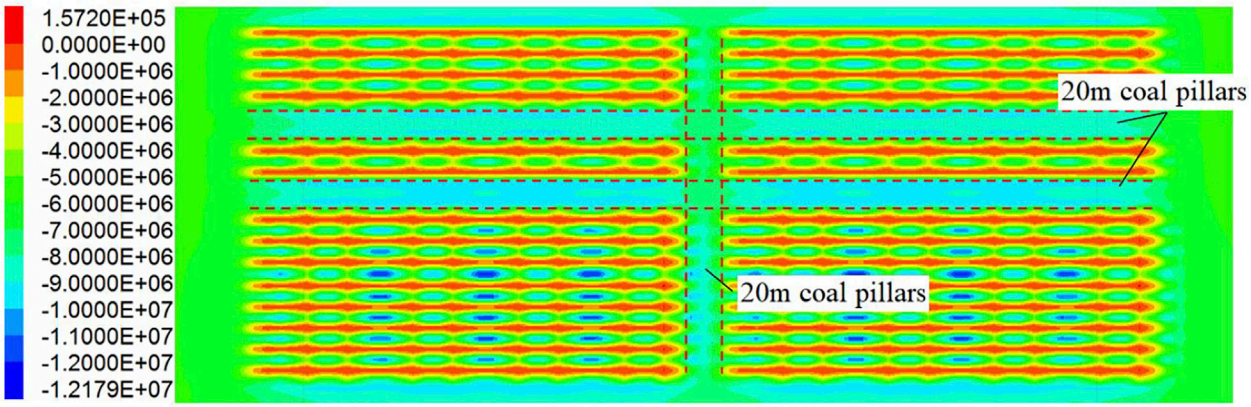

FIGURE 9
Vertical stress distribution of strata at 4 m on top of 3# coal seam (Pa).

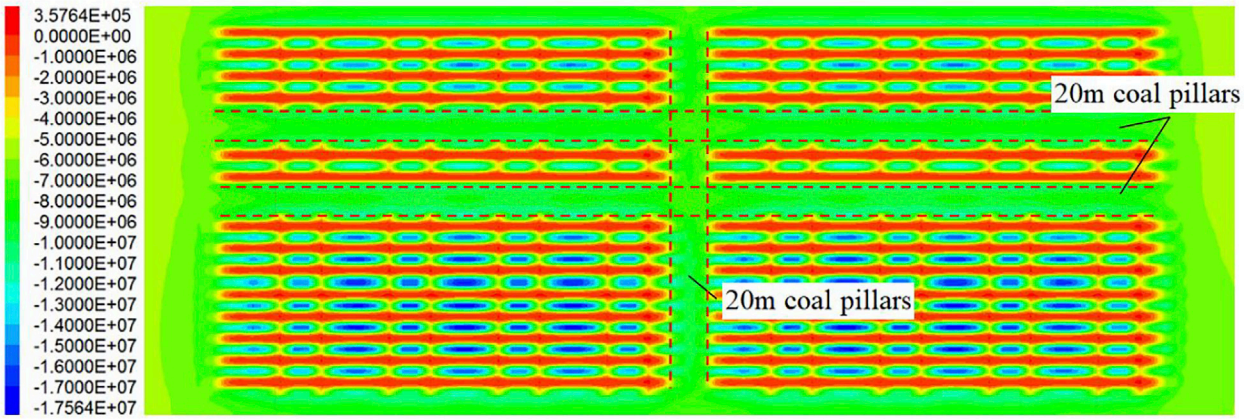

FIGURE 10
Vertical stress distribution of strata at 6m on top of 3# coal seam (Pa).

concentrated coal pillar is 7.0–9.46 MPa, the vertical stress of raw rock is 5.11 Mpa, and the stress concentration coefficient reaches 1.37–1.85. The vertical stress of the surrounding rock under the chamber column is 5.5–8.5 MPa, and the stress concentration coefficient is 1.08–1.67.

Figure 15 shows the cloud diagram of vertical stress distribution at 16m above the roof of a 3# coal seam. Figure 9 shows that the vertical stress of surrounding rock overlying a concentrated coal pillar is 7–8.58 MPa, the vertical stress of raw rock is 5.06MPa, and the stress concentration coefficient reaches 1.38–1.7. The vertical stress of the surrounding rock overlying the room pillar is 5.5–7.5 MPa, and the stress concentration coefficient is 1.09–1.48.

Figure 16 shows the cloud diagram of vertical stress distribution at 18m above the roof of 3# coal seam. Figure 16 shows that the vertical stress of surrounding rock overlying a concentrated coal pillar is 6.5–8.21MPa, the vertical stress of raw rock is 5.01 MPa, and the stress concentration coefficient reaches 1.30–1.64. The vertical stress of the surrounding rock overlying the room pillar is 5.5–7.5 MPa, and the stress concentration coefficient is 1.10–1.30.

Figure 17 shows the cloud diagram of vertical stress distribution at 20m above the roof of 3# coal seam. Figure 10 shows that the vertical stress of surrounding rock overlying a concentrated coal pillar is 6–7.94MPa, the vertical stress of raw rock is 4.96MPa, and the stress concentration coefficient is 1.21–1.6. The vertical stress of the surrounding rock overlying the room pillar is 5.5–6MPa, and the stress concentration coefficient is 1.11–1.21.

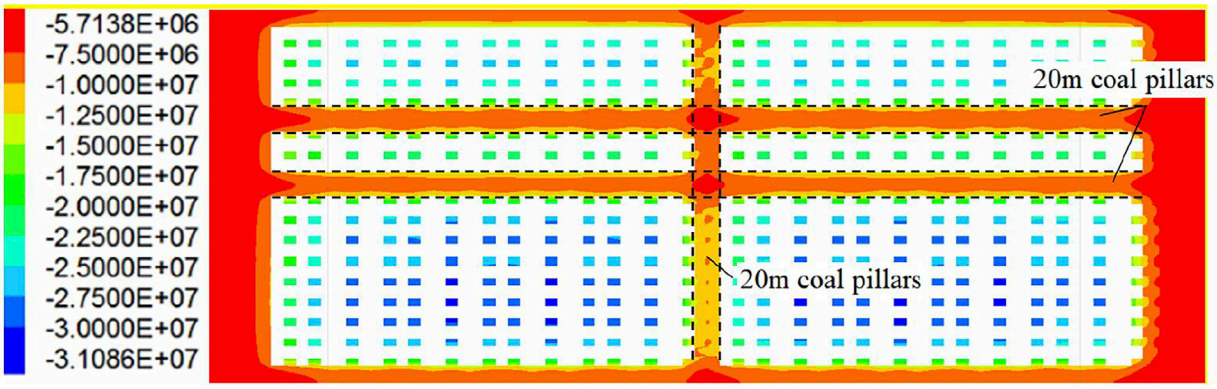

FIGURE 11
Vertical stress distribution of strata at 8m on top of 3# coal seam (Pa).

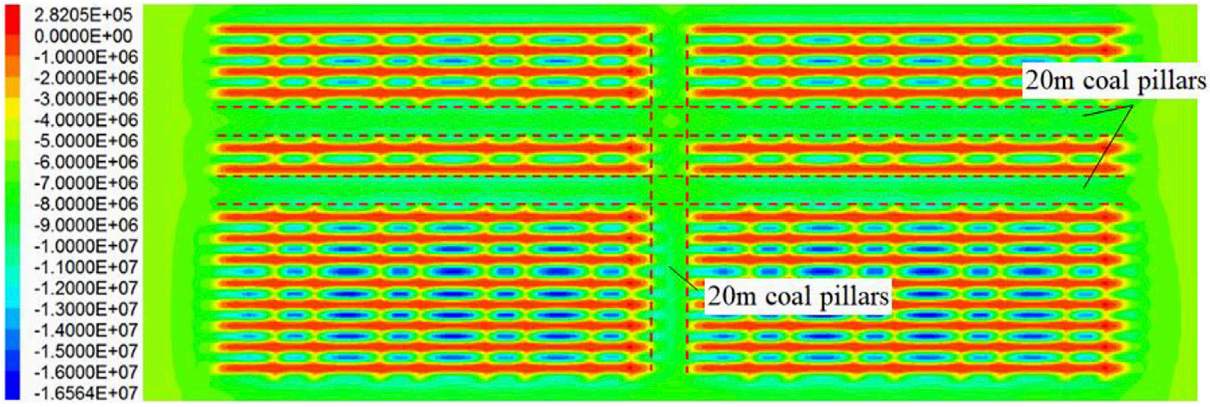

FIGURE 12
Vertical stress distribution of strata at 10m on top of 3# coal seam (Pa).

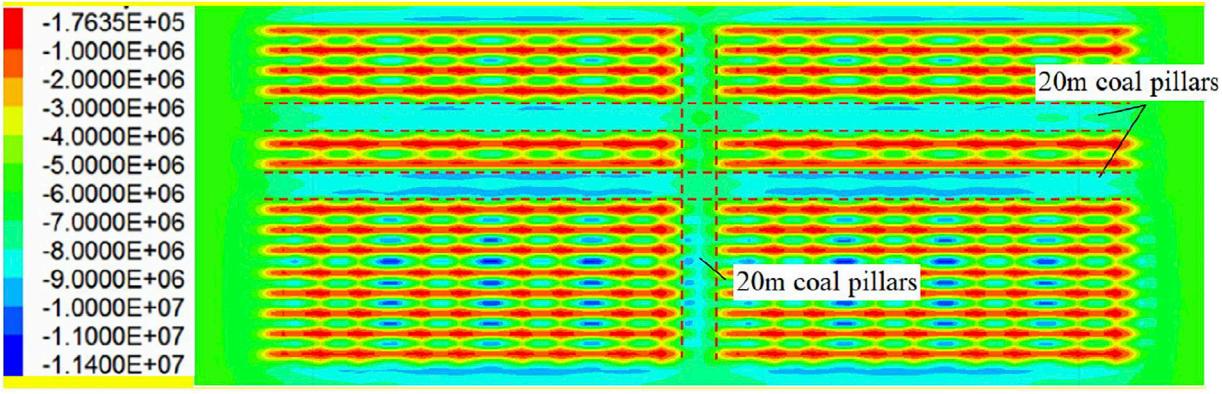

FIGURE 13
Vertical stress distribution of strata at 12m on top of 3# coal seam (Pa).

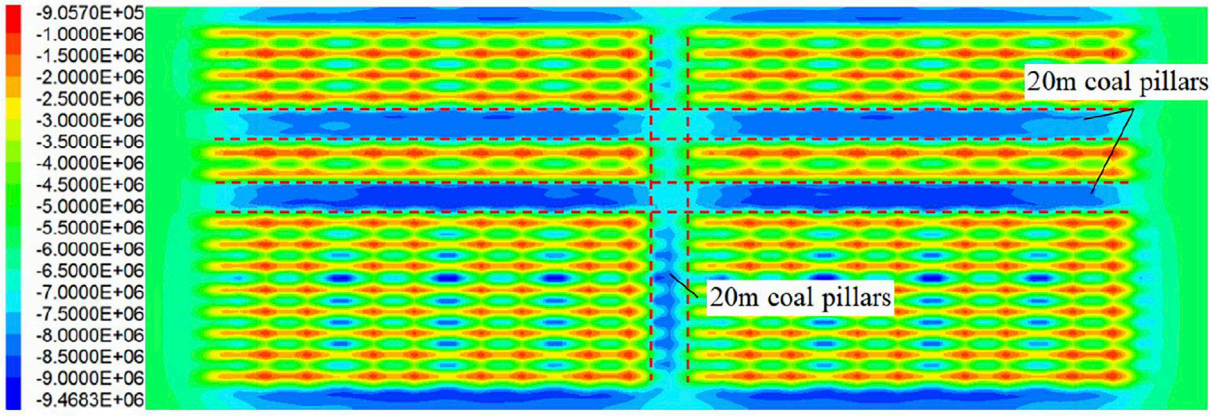

FIGURE 14
Vertical stress distribution of strata at 14m on top of 3# coal seam (Pa).

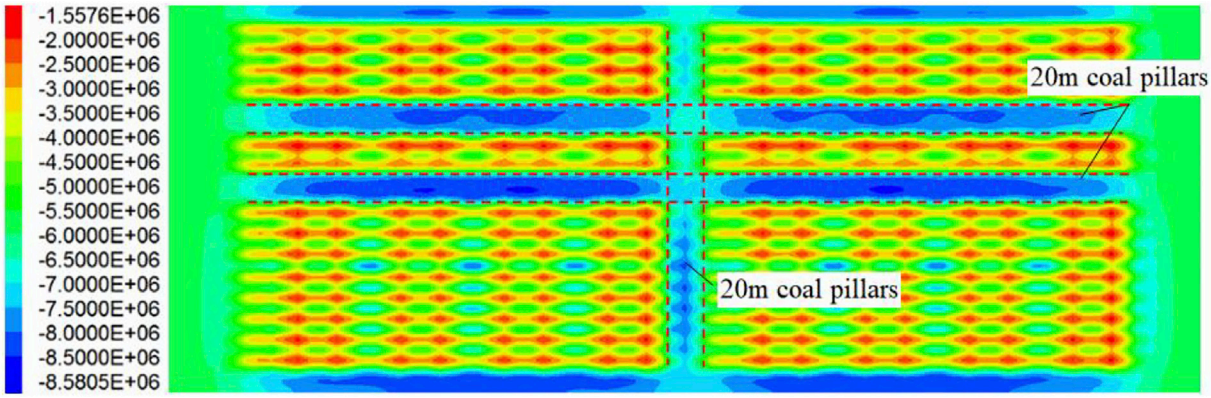

FIGURE 15
Vertical stress distribution of strata at 16m on top of 3# coal seam (Pa).

Advance stress distribution law of working face in 3# coal seam

Figure 18 shows the vertical stress distribution cloud diagram when the 3104 working face is 90m away from the overlying coal pillar. 3# coal seam is affected by the overlying 2–2# coal mining. When the working face of a 3# coal seam is excavated, the superimposed area of mining stress will appear in front of the working face. When 3104's working face is 90 m away from the overlying residual coal, the maximum vertical stress of the residual coal pillar is about 8.98 MPa, while before 3104's working face is mined, the maximum vertical stress of the residual coal pillar is about 8.55 MPa, and the stress concentration coefficient is 1.05.

Figure 19 shows the vertical stress distribution cloud diagram when 3104 working face is 70m away from the overlying coal pillar. When the distance between the 3104 working face and the overlying coal pillar is 70m, the maximum vertical stress of the remaining coal pillar is about 9.21 MPa. Compared with the maximum vertical stress of the remaining coal pillar before mining (8.55 MPa), the stress concentration coefficient is 1.08.

Figure 20 shows the vertical stress distribution cloud diagram when the 3104 working face is 50 m away from the overlying coal pillar. When the distance between the 3104 working face and the overlying coal pillar is 50m, the maximum vertical stress of the remaining coal pillar is about 9.51 MPa. Compared with the maximum vertical stress of the remaining coal pillar before mining (8.55 MPa), the stress concentration coefficient is 1.11.

Figure 21 shows the vertical stress distribution cloud diagram when the 3104 working face is 40m away from the overlying coal pillar. When the distance between the 3104 working face and the overlying coal pillar is 40 m, the maximum vertical stress of the

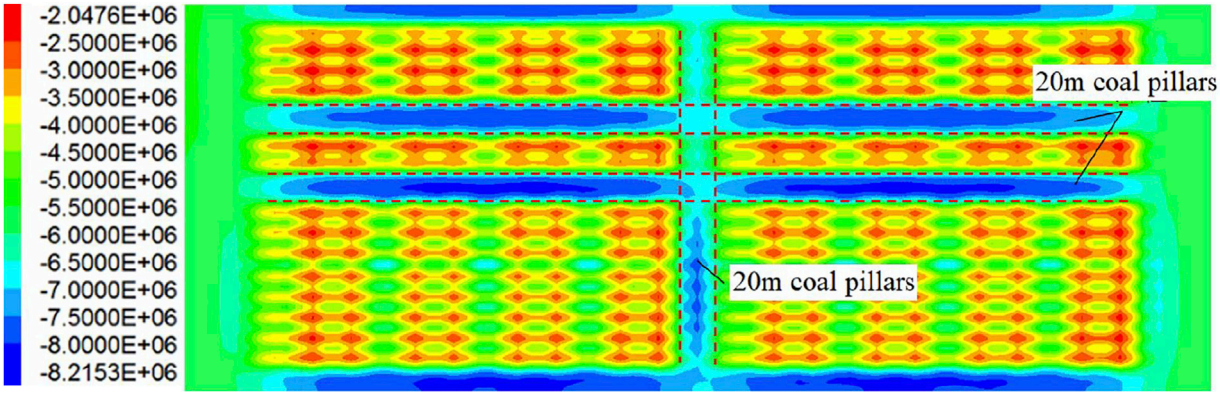

FIGURE 16
Vertical stress distribution of strata at 18m on top of 3# coal seam (Pa).

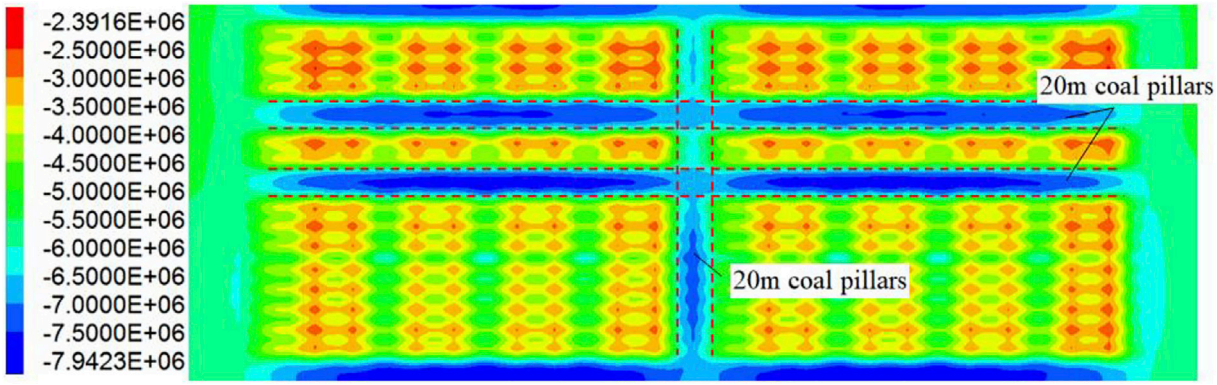

FIGURE 17
Vertical stress distribution of strata at 20m on top of 3# coal seam (Pa).

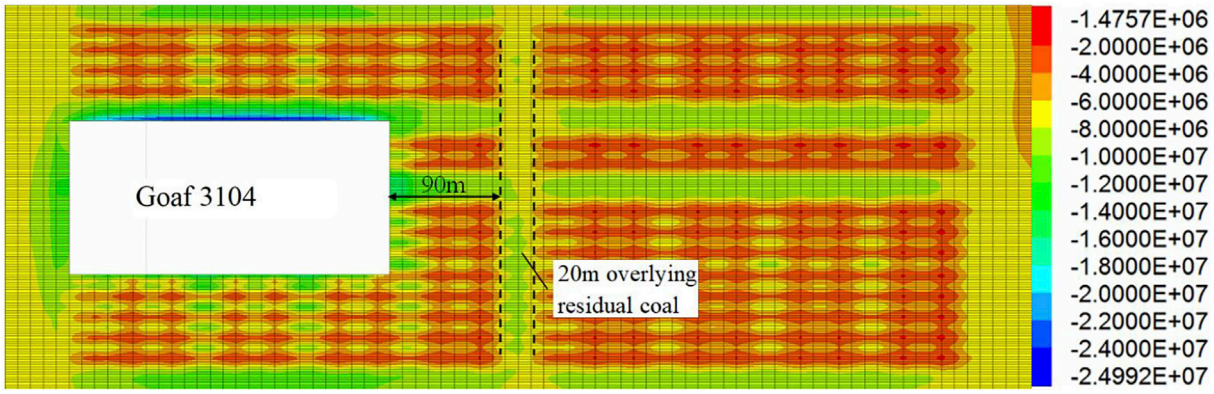

FIGURE 18
Cloud diagram of vertical stress distribution at 90m of overlying residual coal pillar (Pa).

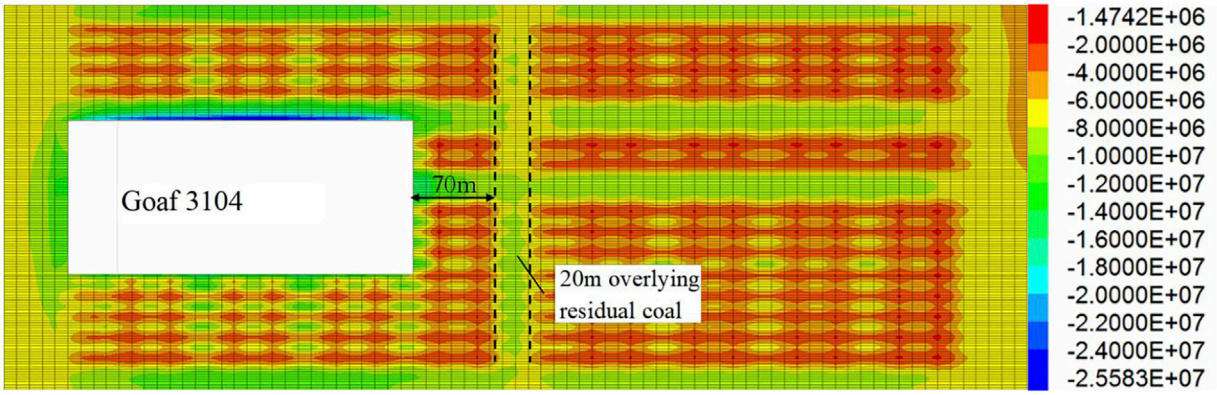

FIGURE 19
Cloud diagram of vertical stress distribution at 70m of overlying residual coal pillar (Pa).

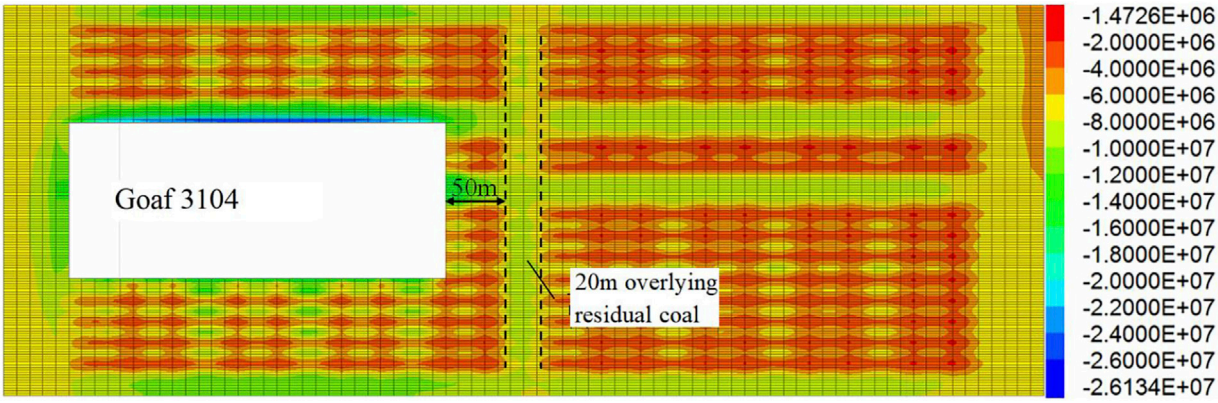

FIGURE 20
Cloud diagram of vertical stress distribution at 50m of overlying residual coal pillar (Pa).

remaining coal pillar is about 9.66 MPa. Compared with the maximum vertical stress of the remaining coal pillar before mining (8.55 Mpa), the stress concentration coefficient is 1.13.

Figure 22 shows the vertical stress distribution cloud diagram when 3104 working face is 30m away from the overlying coal pillar. When the distance between the 3104 working face and the overlying coal pillar is 30 m, the maximum vertical stress of the remaining coal pillar is about 10.24 Mpa. Compared with the maximum vertical stress of the remaining coal pillar before mining (8.55 Mpa), the stress concentration coefficient is 1.2.

Figure 23 shows the vertical stress distribution cloud diagram when the 3104 working face is 20m away from the overlying coal pillar. When the distance between the 3104 working face and the overlying coal pillar is 20m, the maximum vertical stress of the remaining coal pillar is about 10.24 MPa. Compared with the maximum vertical stress of the remaining coal pillar before mining (8.55 MPa), the stress concentration coefficient is 1.2.

Figure 24 shows the vertical stress distribution cloud diagram when the 3104 working face is 10 m away from the overlying coal pillar. When the distance between the 3104 working face and the overlying coal pillar is 10 m, the maximum vertical stress of the remaining coal pillar is about 10Pa. Compared with the maximum vertical stress of the remaining coal pillar before mining (8.55 MPa), the stress concentration coefficient is 1.17.

According to the above numerical simulation analysis, the main results can be summarized. After the room-pillar mining of the 2–2# coal seam, the stress concentration appears in the range of 0–20m in the overlying rock of the 3# coal seam under the influence of the overlying coal pillar. At the top of 3# coal seam, the vertical stress concentration coefficient can reach 2 in the range of 4–12 m, and the vertical stress increases greatly. When 3104 working face pushes 90m in front of the left coal pillar, the vertical stress at the left coal pillar begins to increase, and the influence of advanced mining of 3104 working face begins to

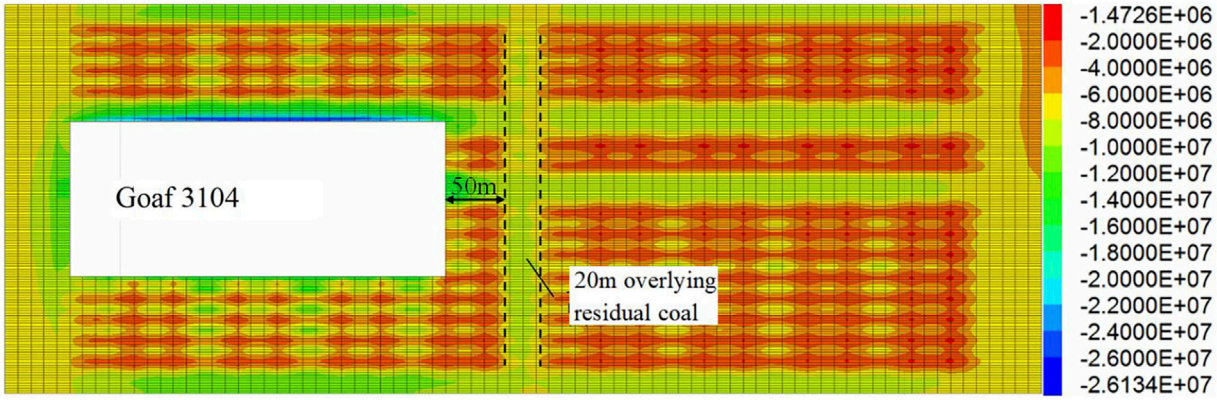

FIGURE 21
Cloud diagram of vertical stress distribution at 40m of overlying residual coal pillar (Pa).

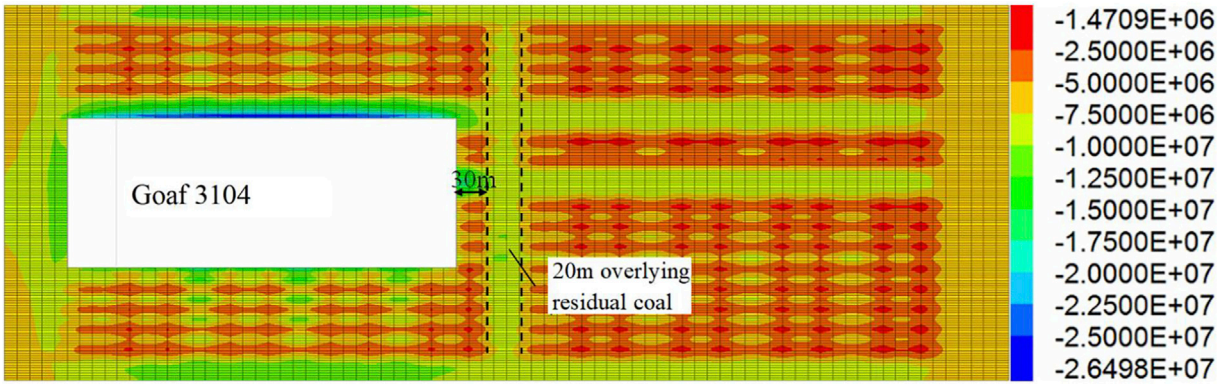

FIGURE 22
Cloud diagram of vertical stress distribution at 30m of overlying residual coal pillar (Pa).

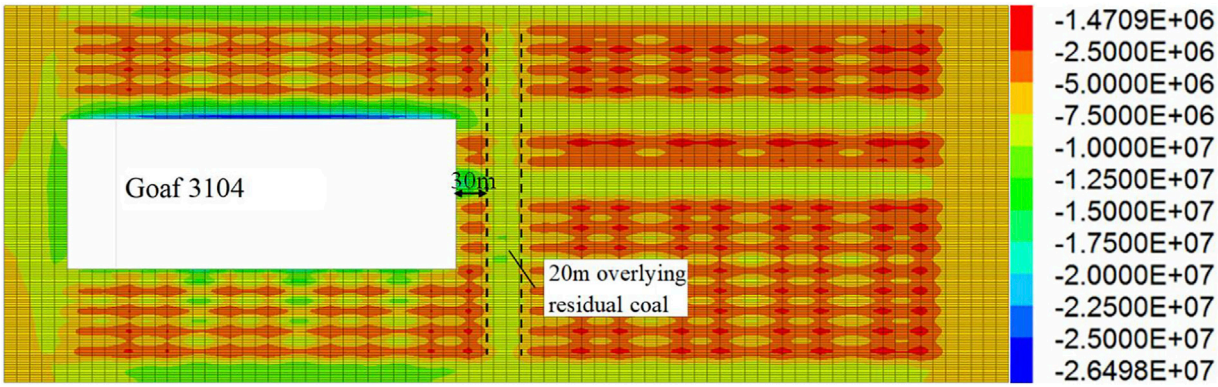

FIGURE 23
Cloud diagram of vertical stress distribution at 20m of overlying residual coal pillar (Pa).

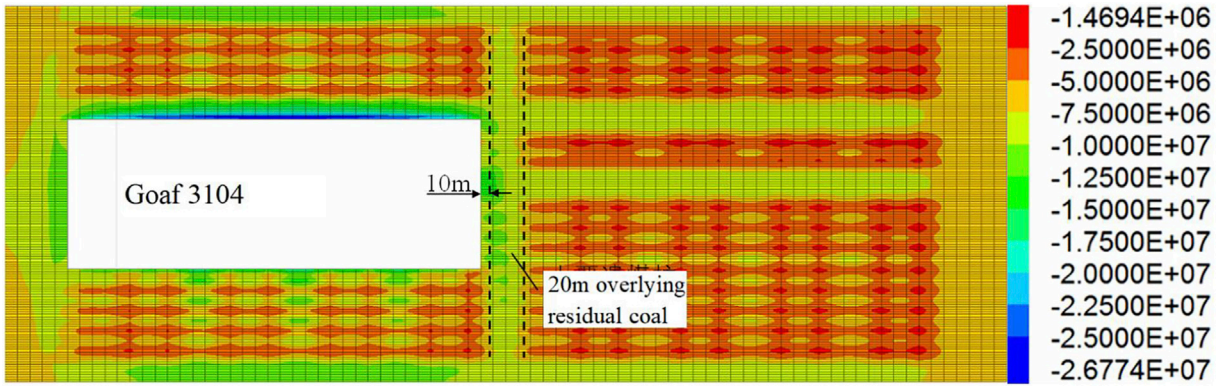

FIGURE 24
Cloud diagram of vertical stress distribution at 10m of overlying residual coal pillar (Pa).

spread to the left coal pillar area. With the advance of the working face, the vertical stress at the remaining coal pillar gradually increases, resulting in the apparent ore pressure on the working face.

Conclusion

1) There are three high-wave velocity stress concentration zones in 280–380 m of 3104 return air roadway, and two high-wave velocity stress concentration zones in 285–340 m of transportation roadway. Because 3104 return air roadway is affected by the stress of the coal pillar in the goaf of the overlying 2–2# coal seam and the side goaf of 3102, while 3104 transport roadway is only affected by the goaf of 3102 working face.
2) The mining of panel 3104 under three mined-out conditions has caused a large mining influence range. There are many microseismic events at 160 m above, 150 m below, and 200 m ahead of the working face. However, the influence of coal pillar concentration stress in the upper 2# coal seam goaf is greater than that in the lower 7# coal seam goaf, which shows that the number of microseismic events above the 3# coal seam is greater than that below the coal seam.3104.
3) After the room-pillar mining of 2–2# coal seams, the overburden rock of 3# coal seams appear to have a high-stress concentration in the range of 0–20 m under the influence of the overburden remaining coal pillar. The vertical stress concentration coefficient of overlying rock in the range of 4–12 m in a no.3 coal seam can reach 2. When the working face is pushed 90 m away from the coal pillar, the vertical stress at the remaining coal pillar begins to increase.
4) Panel 3104 was mined under the condition of three mined-out areas distributed around it, therefore the mining process of 3104 working face is mainly affected by the concentrated coal pillar in the goaf of overlying coal seam. It can be used as a reference for similar working face mining in the Datong mining area.

Data availability statement

The original contributions presented in the study are included in the article/supplementary material; further inquiries can be directed to the corresponding author.

Author contributions

WY: conceptualization, project administration, writing-original draft; ZB: data curation, methodology, DZ: investigation; LK: resources, supervision; WH: validation.

Conflict of interest

The authors declare that the research was conducted in the absence of any commercial or financial relationships that could be construed as a potential conflict of interest.

Publisher's note

References

Chai, J., Wang, R. P., Du, W. G., Lei, W. L., and Zhu, X. B. (2020). Study on time series prediction of rock pressure by XGBoost in optical fiber monitoring[J]. *J. Min. Strata Control Eng.* 2 (04), 64–71. doi:10.13532/j.jmsce.cn10-1638/td.20210607.002

Du, J., and Huang, Q. (2022). Overburden structure evolution and coal pillar stability analysis with different offset distance of coal pillars in shallow multi-seam [J]. *J. Min. Strata Control Eng.* 4 (01), 16–24. doi:10.13532/j.jmsce.cn10-1638/td.20211122.001

Feng, Y. F., Zhao, J., and Wang, C. (2014). Distribution law of floor stress in shortdistance coal seam excavation[J]. *Saf. Coal Mines* 45 (07), 30–33. doi:10.13347/j.cnki.mkaq.2014.07.009

Fu, W. H., Deng, K. Z., and Zhang, L. Y. (2011). Stability analysis of pillar in room-pillar goaf [J]. *Saf. Coal Mines* 42 (01), 136–139. doi:10.13347/j.cnki.mkaq.2011.01.002

Gao, F. Q. (2019). Use of numerical modeling for analyzing rock mechanic problems in underground coal mine practise [J]. *J. Min. Strata Control Eng.* 1 (02), 21–28. doi:10.13532/j.jmsce.cn10-1638/td.2019.02.009

Jiang, L. S., Zhang, P. P., Chen, L. J., Hao, Z., Sainoki, A., Mitri, H. S., et al. (2017). Numerical approach for goaf-side entry layout and yield pillar design in fractured ground conditions. *Rock Mech. Rock Eng.* 50 (11), 3049–3071. doi:10.1007/s00603-017-1277-0

Kai, Z., Tianhong, Y., Haibo, B., and Gamage, R. P. (2017). Longwall mining–induced damage and fractures: Field measurements and simulation using FDM and DEM coupled method[J]. *Int. J. Geomechanics* 18 (1), 1–19. 04017127.

Kong, L. H., Li, Feng, Ouyang, , and Zhenhua, (2016). Study on microseismic monitoring and measuring of fracture distribution features in mining overburden strata [J]. *Coal Sci. Technol.* 44 (01), 109–113. doi:10.13199/j.cnki.cst.2016.01.018

Li, J., Li, X., Liu, C., and Zhang, N. (2022). Study on the air leakage characteristics of a goaf in a shallow coal seam and spontaneous combustion prevention and control strategies for residual coal. *Plos one* 17 (6), e0269822–830. doi:10.1371/journal.pone.0269822

Li J. Z., J. Z., Ti, Z., Zhang, F., Hu, J., and Zhu, Z. (2020). Research on failure characteristics of goaf floor in the inclined coal seam based on the fracture mechanics[J]. *SN Appl. Sci.* 2 (12), 1–6. doi:10.1007/s42452-020-03877-7

Li, J. Z., Yin, Z. Q., and Li, Y. (2019). Waste rock filling in fully mechanized coal mining for goaf-side entry retaining in thin coal seam[J]. *Arabian J. Geosciences* 12 (16), 1–11. doi:10.1007/s12517-019-4650-3

Li, Z., Feng, G., and Cui, J. (2020). Research on the influence of slurry filling on the stability of floor coal pillars during mining above the room-and-pillar goaf: A case study. *Geofluids* 2020 (12), 1–21. doi:10.1155/2020/8861348

Liang, D. (2017). Application of PASAT-M CT scanning in rock burst risk evaluation of Nanshan Coal Mine [J]. *Coal Eng.* 49 (08), 99–102. doi:10.11799/ce201708028

Lin, M. D., Zong, L. M., Zhen, L. L., Cao, A., and Gong, S. (2014). Research progress of monitoring, forecasting, and prevention of rockburst in underground coal mining in China[J]. *Int. J. Coal Sci. Technol.* 1 (3), 278–288. doi:10.1007/s40789-014-0044-z

Liu, W. Z., Guo, Z., Hou, J., and Chen, D. (2019). Research and application of support technology for Re-mining roadway in goaf under regenerated roof in thick coal seam. *Geotech. Geol. Eng. (Dordr).* 37 (5), 4327–4335. doi:10.1007/s10706-019-00910-4

Meng, D., Wang, J., and Wang, J. (2007). Mechanism on the failure and caving of roof strata in pillar and house mining [J]. *J. China Coal Soc.* 32 (06), 577–580. doi:10.3321/j.issn:0253-9993.2007.06.005

Song, J. F., Lu, C. P., Li, Z. W., Ouyang, G. C., Cao, X. M., and Zhou, F. L. (2021). Characteristics of stress distribution and microseismic activity in rock parting occurrence area [J]. *J. Min. Strata Control Eng.* 3 (04), 120–128. doi:10.13532/j.jmsce.cn10-1638/td.20210607.002

Tu, S. H., Dou, F. J., MO, Z. J., Wang, F. T., and Yuan, Y. (2011). Strata control technology of the fully mechanized face in shallow coal seam close to the above room-and-pillar gob [J]. *J. China Coal Soc.* 36 (03), 366–370. doi:10.13225/j.cnki.jccs.2011.03.015

Wang, J. C. (2019). Sustainable coal mining based on mining ground control[J]. *J. Min. Strata Control Eng.* 1 (02), 40–47. doi:10.13532/j.jmsce.cn10-1638/td.2019.02.003

Wang, J. (2022). RNA releases CTCF from chromatin. *Nat. Cell. Biol.* 24, 1. doi:10.1038/s41556-021-00828-1

Wang, Y., Fu, X., Li, F., Liu, W. Y., Zhang, B., and Li, S. G. (2016). Occurrence mechanism of abnormal pressure with mining under instability pillar of room and pillar goaf [J]. *Coal Min. Technol.* 21 (04), 103–106. doi:10.13532/j.cnki.cn11-3677/td.2016.04.027

Wang, Y., Tu, M., Fu, B., and Bu, Q. W. (2020). Study on the distribution of side abutment pressures and ground support for double-used entries in deep mining [J]. *J. Min. Strata Control Eng.* 2 (03), 40–47. doi:10.13532/j.jmsce.cn10-1638/td.20200518.001

Xie, X. Z. (2014). Study on Stability of roof-coal pillar in room and pillar mining goaf in shallow depth seam[J]. *Coal Sci. Technol.* 42 (07), 1–4. doi:10.13199/j.cnki.cst.2014.07.001

Xue, Y., Xu, T., Wasantha, P. L. P., Yang, T. h., and Fu, T. f. (2020). Dynamic disaster control of backfill mining under thick magmatic rock in one side goaf: A case study. *J. Cent. South Univ.* 27 (9), 3103–3117. doi:10.1007/s11771-020-4532-6

Yang, H., Han, C., Zhang, N., Sun, C., Pan, D., and Dong, M. (2019). Stability control of a goaf-side roadway under the mining disturbance of an adjacent coal working face in an underground mine. *Sustainability* 11 (22), 6398. doi:10.3390/su11226398

Yu, D., Yi, X., Liang, Z., Lou, J., and Zhu, W. (2021). Research on strong ground pressure of multiple-seam caused by remnant room pillars undermining in shallow seams. *Energies* 14 (17), 5221. doi:10.3390/en14175221

Yu, Y., Bai, J., Wang, X., and Zhang, L. (2020). Control of the surrounding rock of a goaf-side entry driving heading mining face. *Sustainability* 12 (7), 2623. doi:10.3390/su12072623

Zhang, Y., Wan, Z., Li, F., Zhou, C., Zhang, B., Guo, F., et al. (2013). Stability of coal pillar in gob-side entry driving under unstable overlying strata and its coupling support control technique[J]. *Int. J. Min. Sci. Technol.* 23 (2), 193–199. doi:10.1016/j.ijmst.2013.04.020

Zhang, M. G., Zhang, P., Wang, R., Chen, H., and Kong, P. (2018). Numerical analysis of air leakage characteristics of coal seam goaf close to thin band [J]. *Geotech. Geol. Eng. (Dordr).* 36 (5), 3149–3158. doi:10.1007/s10706-018-0526-7

Zhou, X., Yang, Y., Zheng, K., Miao, G., Wang, M., and Li, P. (2020). Study on the spontaneous combustion characteristics and prevention technology of coal seam in overlying close goaf[J]. *Combust. Sci. Technol.* 194 (5), 1–22. doi:10.1080/00102202.2020.1863953